Accepted Manuscript

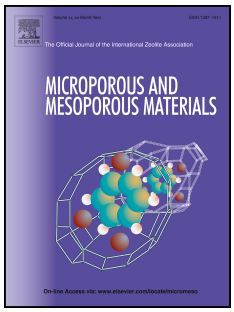

Soft-templated synthesis of mesoporous nickel oxide using poly(styrene-*block*-acrylic acid-*block*-ethylene glycol) block copolymers

Hamzeh Qutaish, Shunsuke Tanaka, Yusuf Valentino Kaneti, Jianjian Lin, Yoshio Bando, Abdulmohsen Ali Alshehri, Shin-Ichi Yusa, Yusuke Yamauchi, Md Shahriar A. Hossain, Jeonghun Kim

PII: S1387-1811(18)30259-2

DOI: 10.1016/j.micromeso.2018.05.015

Reference: MICMAT 8917

To appear in: *Microporous and Mesoporous Materials*

Received Date: 7 March 2018

Revised Date: 30 April 2018

Accepted Date: 12 May 2018

Please cite this article as: H. Qutaish, S. Tanaka, Y.V. Kaneti, J. Lin, Y. Bando, A.A. Alshehri, S.-I. Yusa, Y. Yamauchi, M.S.A. Hossain, J. Kim, Soft-templated synthesis of mesoporous nickel oxide using poly(styrene-*block*-acrylic acid-*block*-ethylene glycol) block copolymers, *Microporous and Mesoporous Materials* (2018), doi: 10.1016/j.micromeso.2018.05.015.

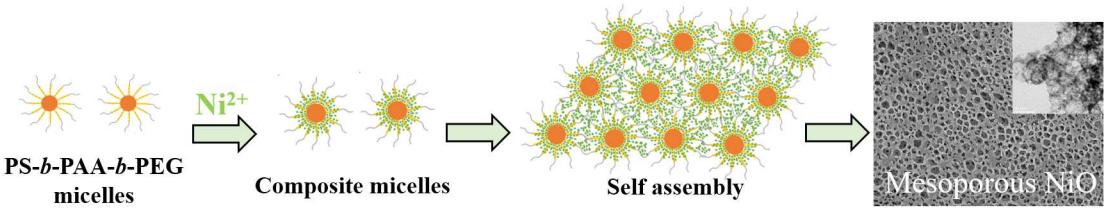

Soft-Templated Synthesis of Mesoporous Nickel Oxide Using Poly(styrene-*block*-acrylic acid-*block*-ethylene glycol) Block Copolymers

Hamzeh Qutaish,[+,1,2] Shunsuke Tanaka,[+,1] Yusuf Valentino Kaneti,*[3] Jianjian Lin,[1] Yoshio Bando[2,3], Abdulmohsen Ali Alshehri,[4] Shin-Ichi Yusa,[5] Yusuke Yamauchi,[6,7] Md. Shahriar A. Hossain*[8] and Jeonghun Kim*[6]

1 College of Chemistry and Molecular Engineering, Qingdao University of Science and Technology, Qingdao 266042, China

2 Australian Institute of Innovative Materials (AIIM), University of Wollongong, North Wollongong, New South Wales 2500, Australia

3 International Center for Materials Nanoarchitectonics (WPI-MANA), National Institute for Materials Science (NIMS), 1-1 Namiki, Tsukuba, Ibaraki 305-0044, Japan

4 Department of Chemistry, King Abdulaziz University, P.O. Box. 80203, Jeddah 21589, Saudi Arabia

5 Department of Applied Chemistry, University of Hyogo, Himeji, 2167 Shosha, Himeji 671-2280, Japan.

6 School of Chemical Engineering & Australian Institute for Bioengineering and Nanotechnology (AIBN), The University of Queensland, Brisbane, QLD 4072, Australia

7 Department of Plant & Environmental New Resources, Kyung Hee University, 1732 Deogyeong-daero, Giheung-gu, Yongin-si, Gyeonggi-do 446-701, South Korea.

8 School of Mechanical & Mining Engineering, The University of Queensland, Brisbane, QLD 4072, Australia

+ These authors equally contributed to this work.

E-mails: KANETI.Valentino@nims.go.jp; shahriar@uow.edu.au; jeonghun.kim@uq.edu.au

Keywords: Mesoporous materials; Nickel oxide; Block copolymers; Soft-templates; Metal oxides

Abstract

In this work, we report the soft-templated preparation of mesoporous nickel oxide using an asymmetric poly(styrene-*block*-acrylic acid-*block*-ethylene glycol) (PS-*b*-PAA-*b*-PEG) triblock copolymer. This block copolymer forms a micelle consisting of a PS core, a PAA shell and a PEG corona in aqueous solutions, which can serve as a soft template. Specifically, the PS block forms the core of the micelles on the basis of its lower solubility in water. The anionic PAA block interacts with the cationic Ni^{2+} ions present in the solution to generate the shell. The PEG block forms the corona of the micelles and stabilizes the micelles by preventing secondary aggregation through steric repulsion between the PEG chains. In terms of textural characteristics, the as-synthesized mesoporous NiO exhibits a large average pore size of 35 nm with large specific surface area and pore volume of 97.0 m^2 g^{-1} and 0.411 cm^3 g^{-1}, respectively. It is expected that the proposed soft-templated strategy can be expanded to other metal oxides/sulfides in the future for potential applications in gas sensors, catalysis, energy storage and conversion, optoelectronics, and biomedical applications.

1. Introduction

Over the past decades, porous materials have gained significant interests for various applications, such as energy storage and conversion, sensors, catalysis, biomedical and optoelectronics due to their high surface area, large pore volume and porosity, tunable pore size, *etc*.[1,2] Among various types of porous materials, mesoporous materials (materials with pore sizes between 2-50 nm) have attracted the most attention owing to their uniform pore size, rich surface chemistry, controllable wall composition, and modifiable surface properties.[3,4] In particular, mesoporous transition metal oxides are highly attractive for a wide range of applications, including chemical, environmental/energy, optics, electronics, medical, and biotechnological applications.[5-7]

In general, mesoporous transition metal oxides are synthesized by using two approaches: hard and soft-templating methods.[8] In hard-templating method, suitable metal precursors are firstly introduced into the pores of mesoporous templates and subsequent heating results in the desired crystalline metal oxides and selective removal of the template generates the mesoporous metal oxide replica.[9] The pore size, wall thickness, and topological structure of the resulting mesoporous metal oxide replica could be controlled to some extent by correspondingly changing those of their templates. To date, many different mesoporous metal oxides (including transition metal oxides) have been reported using the hard-templating (nanocasting) method, including TiO_2,[10] MnO_2,[11,12] Fe_3O_4,[13] Fe_2O_3,[13] Co_3O_4,[11,14] Al_2O_3,[15] and WO_{3-x}.[16] However, there are some disadvantages associated with the hard-templating method, such as long and complex procedures, difficulties to fill in the mesoporous silica template due to complex interactions between the silica and filtrated metal ion precursor, and the use strong acid (*e.g.*, hydrofluoric acid (HF)) to remove the hard template.[9]

On the other hand, soft-templating methods typically employ surfactants or block copolymers. The synthesis of mesoporous metal oxides by soft-templating method offers many advantages, including lower cost of the template, simpler procedures which can be carried out under mild conditions, and tunable pore size and chemical composition.[8] However, these methods also have some drawbacks as their syntheses are often based on complicated so-gel processes, as well as the hydrolysis and polymerization of transitional metal species which are difficult to control. Furthermore, the resulting mesoporous oxide products tend to

exhibit amorphous or semi-crystalline walls and poor thermal stability. Triblock copolymers have previously been employed as soft-templates to synthesize mesoporous transition metal oxides with small pore sizes.[17] For instance, Yang *et al.* have reported the synthesis of mesoporous TiO_2 with an average pore size of smaller than 10 nm by using the PEO-*b*-PPO-*b*-PEO type block copolymer.[18] However, mesoporous materials with such small pores may have limited applications compared to those with larger pores as they may not be able to accommodate large guest species or molecules.

Recently, many efforts have been carried out to enlarge the pore size of mesoporous materials.[17] The utilization of block copolymers which possess long hydrophobic block could overcome this challenge because the pore size strongly relies on hydrophobic block length of the micelle template. Previously, our group reported the use of high molecular weight diblock copolymers, such as polystyrene-*block*-poly(ethylene oxide) (PS-*b*-PEO) as soft-templates for the preparation of mesoporous materials with large pore size.[19,20] Furthermore, we have also synthesized mesoporous nickel ferrite and ferrite with large pore sizes through the use of poly(styrene-*block*-acrylic acid-*block*-ethylene glycol) (PS-*b*-PAA-*b*-PEG) triblock copolymer containing acrylic acid (negatively charged in alkaline solutions).[21,22]

Among various metal oxides, nickel oxide (NiO), a wide bandgap (3.6-4.0 eV) *p*-type semiconductor has gained significant attention due to its exciting intrinsic properties, such as electrochromic, antiferromagnetic, and high capacitive properties.[23-25] In addition, NiO can be utilized in a wide range of applications, including electrochromic display devices, smart windows, active optical fibers, gas sensors, solar thermal absorbers, catalysis, fuel cell electrodes, supercapacitors, and energy storage.[23-25] To date, many previous reports on mesoporous NiO relied on the use of hard templates, such as SBA-15[26] and KIT-6.[27,28] Despite some progress, reports on the fabrication of mesoporous NiO using soft-templates are still scarce.

In this study, we report the synthesis of mesoporous NiO with a large average pore size of 35 nm by utilizing PS-*b*-PAA-*b*-PEG triblock copolymer as a soft-template (**Figure 1**). In aqueous solution, the PS-*b*-PAA-*b*-PEG block polymer forms tri-functional micelles, in which the PS, PAA and PEG blocks act as

core, shell, and corona, respectively. The effects of nickel precursor amount and calcination temperature were investigated to determine the optimum condition for achieving well-defined mesoporous NiO.

2. Experimental Section

2.1. Chemicals.

Poly(ethylene glycol) methylether (4-cyano-4-pentanoate dodecyl trithiocarbonate) (PEG_{46}-CTA, M_n = 2,400 g mol^{-1}) from Aldrich and 2,2'-azobis (2,4-dimethylvaleronitrile) (V-65, ≥ 95.0%) from Wako Pure Chemical were used as received without further purification. Acryl acid (AA, ≥ 98.0%) and styrene (St, ≥ 99.0%) from Wako Pure Chemical were dried with 4 Å molecular sieves and purified by distillation under reduced pressure. 2,2'-Azobis (2-methylpropionitrile) (AIBN, ≥ 98.0%) from Wako Pure Chemical was purified by recrystallization from methanol. 1,4-Dioxane and methanol were dried with 4 Å molecular sieves and purified by distillation. Water was purified using a Millipore Milli-Q system. Nickel (II) nitrate hexahydrate ($Ni(NO_3)_2 \cdot 6H_2O$, 98%) and absolute ethanol (C_2H_6O, 99.99%) were purchased from Sigma Aldrich and they were used without further purification.

2.2. Preparation of PS_{402}-*b*-PAA_{71}-*b*-PEG_{46} triblock copolymer.

The preparation method of PS_{402}-*b*-PAA_{71}-*b*-PEG_{46} is shown in **Figure 1**. AA (4.95 g, 68.7 mmol), PEG_{46}-CTA (1.10 g, 0.458 mmol), and AIBN (30.1 mg, 0.183 mmol) were dissolved in 1, 4-dioxane (70.0 mL). The solution was degassed by purging with Ar gas for 30 min. Polymerization was performed at 60 °C for 15 h. After the reaction, the conversion of AA estimated from ^{1}H NMR was 40.4%. The reaction mixture was dialyzed against pure water for three days. PAA_{71}-*b*-PEG_{46} was recovered by freeze-drying (2.44 g, 40.4 %). The number-average molecular weight (M_n(NMR)), degree of polymerization (DP) of PAA estimated from ^{1}H NMR, and molecular weight distribution (M_w/M_n) estimated from gel-permeation chromatography (GPC) were 7.52×10^3 g mol^{-1}, 71, and 1.41, respectively (**Table S1**).

PAA_{71}-*b*-PEG_{46} (1.50 g, 0.200 mmol, M_n(NMR) = 7.52×10^3 g mol^{-1}, M_w/M_n = 1.41), St (10.4 g, 99.8 mmol), and V-65 (24.9 mg, 0.100 mmol) were dissolved in methanol (50.0 mL). The solution was degassed by purging with Ar gas for 30 min. Polymerization was performed at 50 °C for 24 h. After the reaction, the conversion of St estimated from ^{1}H NMR was 55.2%. The reaction mixture was dialyzed

against methanol for three days, then pure water for two days. After the dialysis, the aqueous solution of PS_{402}-*b*-PAA_{71}-*b*-PEG_{46} was recovered (362 mL). The polymer powder was recovered from a part of the aqueous polymer solution (20 mL) by freeze-drying with a yield of 0.355 g. The concentration of the aqueous polymer solution was 17.8 g/L. M_n(NMR) of PS_{402}-*b*-PAA_{71}-*b*-PEG_{46} and DP(NMR) of PS estimated from ^{1}H NMR, and M_w/M_n estimated from GPC were 4.94×10^4 g mol^{-1}, 402, and 1.37, respectively (**Table S1**).

2.3. Synthesis of mesoporous nickel oxide

In a typical procedure, 20 mg of nickel (II) nitrate hexahydrate was firstly dissolved in 80 µL of ethanol. After perfect dissolution, this solution was added into 2 mL of polymeric micelles solution (5 g L^{-1}) under magnetic stirring. After stirring for 1 h, the mixture was dried at 60 °C in an electrical oven. The collected light green powder was then calcined at different temperatures (250-450 °C) with a heating rate of 2 ºC min^{-1}.

2.4. Characterization

^{1}H NMR was obtained using a Bruker DRX-500 spectrometer. GPC measurement for PAA_{71}-*b*-PEG_{46} was performed using a Tosoh RI-8020 refractive index detector equipped Shodex 7.0 µm beads size GF-7M HQ column (exclusion limit ~ 10^7) working at 40 °C under a flow rate of 0.6 mL/min. A phosphate buffer (50 mM, pH 9) containing 10 vol% acetonitrile was used as an eluent. The values of M_n and M_w/M_n for the polymers were calibrated using standard sodium poly(styrenesulfonate) samples. GPC measurement for PS_{402}-*b*-PAA_{71}-*b*-PEG_{46} was performed using a Shodex DS-4 pump and an RI-101 refractive index detector using Shodex one KF-805L and three KF803L columns connected in series. THF was used as the eluent at a flow rate of 1.0 mL/min at 40 °C. M_n and M_w/M_n were calibrated using PS standard samples. Sample solutions were filtered with a 0.2 µm pore size membrane filter. Dynamic light scattering (DLS) measurements were performed using a Malvern Zetasizer Nano ZS with a He-Ne laser (4 mW at 633 nm) at 25 °C. The hydrodynamic radius (R_h) was calculated using the Stokes-Einstein equation, $R_h = k_B T/(6\pi\eta D)$, where k_B is Boltzmann constant, T is absolute temperature, and η is solvent viscosity. The DLS data was analyzed using Malvern Zetasizer software version 7.11. Zeta-potential (ζ) was measured using a Malvern Zetasizer Nano-ZS at 25 °C. ζ was calculated from the electrophoretic mobility (μ) using the Smoluchowski

relationship, $\zeta = \eta\mu/\varepsilon$ ($\kappa a >> 1$), where ε is the dielectric constant of the solvent, κ is the Debye-Hückel parameter, and a is particle radius, respectively. TEM observation was performed with a JEOL JEM-2100 operated at an accelerating voltage of 200 kV. The TEM sample was prepared by placing one drop of the aqueous solution on a copper grid coated with a thin film of Formvar. Excess water was blotted using filter paper. The sample was stained by sodium phosphotungstate and dried under vacuum for one day. The morphological observation of the mesoporous NiO was performed using both scanning (SEM; JEOL JSM-7500FA) and transmission electron microscopes (TEM; JEOL JEM-2010). The phase composition and crystal structures of the samples were analyzed by X-ray diffraction (GBC MMA XRD) with Cu-Kα (1.54 Å) in the 2θ range of 10 to 80°. Nitrogen (N_2) adsorption-desorption measurements were performed using a BET Nova 1000 at 77 K. The specific surface areas were calculated using the multipoint Brunauer-Emmett-Teller (BET) method at a relative pressure (P/P_0) range of 0.05 to 0.30, while the total pore volumes were calculated by the Barrett-Joyner-Halenda (BJH) method. Prior to the BET measurements, the samples were degassed under vacuum at 100 °C for overnight. Finally, thermogravimetric analysis (TGA) was carried out using a Mettler Toledo TGA/DTA851 thermal analyzer apparatus with a heating rate of 10 °C min^{-1} in air atmosphere.

3. Result and Discussion

The DP (NMR) for PAA was determined from the integral intensity ratio of the peaks at 3.5 (*a*) and 1.1-1.9 ppm (*e*+*f*) (**Figure S1a**). The DP (NMR) for PS was determined from the integral intensity ratio of the peaks at 1.2-2.5 (*d*+*e*+*h*+*i*) and 6.3-7.2 ppm (*j*+*k*) (**Figure S1b**). The M_n(GPC) values for PEG_{46}-*b*-PAA_{71} and PS_{402}-*b*-PAA_{71}-*b*-PEG_{46} were 1.03×10^4 and 1.43×10^5 g mol^{-1}, respectively (**Figure S2**). M_w/M_n estimated from GPC were relatively narrow below 1.5 (**Table S1**). Theoretical degree of polymerization (DP(theory)) and theoretical number-average molecular weight (M_n(theory)) were calculated from the following equations:

$$DP(theory) = \frac{[M]_o}{[CTA]_o} \times \frac{P}{100} \quad (1)$$

$$M_n(theory) = DP(theory) \times MW + MW_{CTA} \quad (2)$$

where $[M]_0$ is the initial monomer concentration, $[CTA]_0$ is the initial chain transfer agent (CTA) concentration, p is monomer conversion estimated from ^{1}H NMR measurements, MW is the molecular weight of monomer, and MW_{CTA} is the molecular weight of CTA. The values of DP(theory) and M_n(theory) are listed in **Table S1**. DLS measurements for PS_{402}-*b*-PAA_{71}-*b*-PEG_{46} at polymer concentration (C_p) = 0.2 g/L were performed in pure water at pH 5.1 (**Figure S3**). The unimodal distribution with R_h = 58.0 nm can be observed. PAA was ionized in pure water. The zeta-potential of PS_{402}-*b*-PAA_{71}-*b*-PEG_{46} in water at pH 5.1 was -42.8 mV, because the pH value of the aqueous solution was 5.1 which is near to pK_a (= 4.35) of AA monomer. TEM observation for PS_{402}-*b*-PAA_{71}-*b*-PEG_{46} in pure water was performed (**Figure 2a**). An average diameter of 31 nm was estimated from TEM (**Figure 2b**), which was different from R_h (= 58.0 nm) estimated from DLS measurement since the TEM sample was in dried state.

The formation mechanism of the mesoporous nickel oxide using the PS-*b*-PAA-*b*-PEG block copolymer as a soft-template is illustrated in **Figure 3**. In the reaction system, the PS block forms the core of the micelles due to its rigid and glassy structure in water and acts as a pore-forming agent.[21,22] According to zeta-potential, PAA was negatively-charged in the water. After addition of nickel (II) nitrate solution, the pH value was changed to around 4.5. In this pH region, PAA is still negatively-charged, where the negatively-charged PAA block interacted with the positively-charged cationic metal ions and forming the shell.[21,22] In this study, unlike our previous study[21,22], NaOH solution was not used as additive for controlling the pH in the solution. The PEG block forms the corona, which provides stability for the micelles in the solution to prevent secondary aggregation and promote the orderly organization of the particles during assembly of the micelles. The drying of the solution at 60 °C promotes the formation of mesostructured material. Finally, the calcination at high temperatures can lead to cross-linking of the NiO frameworks and simultaneous removal of the polymeric template.

In order to determine the optimized conditions for the synthesis of mesoporous NiO, the effect of different concentration of nickel salt was investigated and the corresponding SEM images are given in **Figure 4**. The use of a low amount of nickel precursor (10 mg, 0.0344 mmol) is found to yield mesoporous structures with a large average pore size of around 36 nm, but with very thin walls (thickness of around 6 nm) and some presence of defects on the wall (**Figures 4a** and **b**). The increase in the amount of the nickel

precursor to 20 mg (0.0688 mmol) gives rise to well-defined mesoporous structures with average pore size and wall thickness of 35 nm and 14 nm, respectively (**Figures 4c** and **d**). However, excess addition of the nickel salt (30 mg, 0.1032 mmol) results in aggregation of the small crystals, thereby leading to the collapse of the mesopores and the corresponding decrease in surface area (**Figures 4e** and **f**). Based on these results, an optimum nickel precursor amount of 20 mg (0.0688 mmol) was used for further experiments.

The effect of the calcination temperature on the morphology of the resulting mesoporous NiO was checked by SEM (**Figure 5**). When the sample was calcined at 250 °C, the mesoporous structure is not observed at all (**Figure 5a**). This is because the temperature was not high enough to remove the carbon components in the PS-*b*-PAA-*b*-PEG block copolymer. In contrast, the increase in calcination temperature to 350 °C leads to the formation of well-defined mesoporous NiO with an average pore size of around 35 nm (**Figure 5b**). However, raising the calcination temperature further to 450 °C causes the collapse of the mesoporous structures as the higher temperature induced by further crystallization of NiO (**Figure 5c**).

The TEM image of the mesoporous NiO obtained at an optimum calcination temperature of 350 °C reveals its well-defined mesoporous structure with average pore and grain sizes of 35 nm and 6 nm, respectively (**Figure 6a**). The pore size of mesoporous NiO was slightly larger than the micelle size of block copolymer (**Figure 2**) because the PEG-PAA shell can also contribute to the formation of pores during reaction. The high-resolution TEM (HRTEM) image of the mesoporous NiO obtained at 350 °C displays well-defined lattice fringes with *d*-spacing of 0.24 nm and 0.20 nm, corresponding to the *d*-spacing of NiO(111) and NiO(200), respectively, as shown in **Figure 6b**. The corresponding selected area electron diffraction (SAED) pattern (Inset of **Figure 6b**) reveals the polycrystalline nature of this mesoporous NiO.

TGA was conducted to analyze the weight changes of pure PS-*b*-PAA-*b*-PEG triblock copolymer and the PS-*b*-PAA-*b*-PEG micelles (containing Ni^{2+}) with increasing temperatures. As shown in **Figure 7a**, the block copolymer undergoes a sharp weight loss beginning at around 200 °C and completely burns out at around 450 °C. On the other hand, for PS-*b*-PAA-*b*-PEG micelles (containing Ni^{2+}), an initial decrease of the TG curve is observed at ~200 °C (~17%), which can be associated with the removal of adsorbed water molecules, whereas the weight loss observed from 200 °C to 370 °C could be attributed to the decomposition of the PS-*b*-PAA-*b*-PEG template, as shown in **Figure 7b**. No further weight loss was

observed after 370 °C, indicating the complete removal of the polymeric template. Therefore, it can be concluded that the calcination process at 350 °C is enough to completely remove the organic template if the applied heating rate is very slow (In our experiment, the heating rate was 2 ºC min^{-1}). These results are in good agreement with the SEM observations.

The XRD patterns of the mesoporous NiO obtained at different calcination temperatures are shown in **Figure 7c**. The observed diffraction peaks can be indexed to the (111) and (200) planes of face-centered cubic NiO phase (JCPDS No. 01-078-0429). Furthermore, it is evident that the diffraction peaks of the mesoporous NiO become narrower and sharper with increasing the calcination temperature. The average crystallite size was calculated from the most intense diffraction peak by using Scherrer's formula.

$$D = 0.94\lambda/(\beta\, cos\theta) \qquad (3)$$

where D is the average crystallite size, β is the broadening of FWHM of the main intense peak (111) in radian, θ is the Bragg angle, and λ is the radiation wavelength. Using the above equation, the average crystallite sizes of the mesoporous NiO obtained at calcination temperatures of 250 °C, 350 °C, and 450 °C are calculated to be 19.5 nm, 27.4 nm, and 36.5 nm, respectively. This trend clearly indicates the increase in average crystallite size with increasing calcination temperature.

The XRD pattern of the mesoporous NiO obtained at 250 °C shows the existence of crystalline NiO; however this temperature is not sufficient to remove the block copolymer template completely, as supported by the TGA data. The increase in calcination temperature of up to 450 °C leads to further improvement in the crystallinity of the mesoporous NiO product, as indicated by the increase in intensity of the NiO(111) peak observed in **Figure 7b** and **c**. The nitrogen adsorption-desorption isotherm of the mesoporous NiO obtained at an optimum calcination temperature of 350 °C is shown in **Figure 7d**. According to the BET analysis, the specific surface area and pore volume of the mesoporous NiO obtained at 350 °C are 97 m^2 g^{-1} and 0.411 cm^3 g^{-1}, respectively.

4. Conclusions

In this report, well-defined mesoporous NiO with large average pore size of 35 nm has been successfully synthesized using PS-*b*-PAA-*b*-PEG block copolymer as a soft-template followed by their removal at an

optimum calcination temperature of 350 °C. In the proposed method, the PS block forms the core of the micelles and functions as a pore-forming agent, whereas the PAA block interacts with cationic Ni ions to form the shell of the micelles due to its strong electrostatic charge, and the PEG block forms the corona of the micelles and provides stability by preventing secondary aggregation before/during micelle assembly. An optimum amount of the nickel precursor is necessary to ensure the formation of well-defined mesoporous NiO. The optimum mesoporous NiO sample exhibits large surface area and pore volume of 97.0 m^2 g^{-1} and 0.411 cm^3 g^{-1}. The excellent textural properties of the synthesized mesoporous NiO may enable it to be utilized as high-performance material in catalysis, gas sensors, energy storage and conversion, and biomedical applications. The large surface area and pore volumes of the mesoporous NiO are expected to be beneficial in enhancing its functional performance for a variety of applications, including energy storage and conversion,[29-32] catalysis,[33-34] gas sensors,[35] and biomedical applications[36]. Furthermore, the proposed soft-templating method can be expanded into other metal oxides or sulfides in the future for obtaining mesoporous oxides/sulfides with enhanced textural characteristics and functional performance.

Conflicts of interest

There are no conflicts to declare

Appendix A. Supplementary data

Supplementary data related to this article can be found at http://dx

Acknowledgement

This work was supported by an Australian Research Council (ARC) Future Fellow FT150100479) and JSPS KAKENHI (Grant Numbers 17H05393 and 17 K19044). Yusuf Valentino Kaneti is an overseas researcher under Postdoctoral Fellowship from the Japanese Society for the Promotion of Science (JSPS). This work was also supported by the Deanship of Scientific Research (DSR), King Abdulaziz University (KEP-7-130-39).

References

[1] C. M. A. Parlett, K. Wilson and A. F. Lee, Chem. Soc. Rev. 2013, 42, 3876-3893.

[2] J. Tang, J. Liu, N. L.Torad, T. Kimura and Y. Yamauchi, Nano Today, 2014, 9, 305-323.

[3] N. Linares, A. M. Silvestre-Albero, E. Serrano, J. Silvestre-Albero and J. Garcia-Martinez, Chem. Soc. Rev. 2014, 43, 7681-7717.

[4] K. Ariga, A. Vinu, Y. Yamauchi, Q. Ji and J. P. Hill, Bull. Chem. Soc. Jpn. 2011, 85, 1-32.

[5] Y. Ren, Z. Ma and P. G. Bruce, Chem. Soc. Rev. 2012, 41, 4909-4927.

[6] D. Gu and F. Schüth, Chem. Soc. Rev. 2014, 43, 313-344.

[7] J. L Vivero-Escoto, Y. D. Chiang, K. C. W. Wu and Y. Yamauchi, Sci. Tech. Adv. Mater. 2012, 13, 013003.

[8] V. Malgras, Q. Ji, Y. Kamachi, T. Mori, F.-K. Shieh, K. C. W. Wu, K. Ariga and Y. Yamauchi, Bull. Chem. Soc. Jpn. 2015, 88, 1171-1200.

[9] B. Tian, X. Liu, H. Yang, S. Xie, C. Yu, B. Tu and D. Zhao, Adv. Mater. 2003, 15, 1370-1374.

[10] Z. Zhang, F. Zuo and P. Feng, J. Mater. Chem. 2010, 20, 2206-2212.

[11] J. Deng, L. Zhang, H. Dai, Y. Xia, H. Jiang, H. Zhang and H. He, J. Phys. Chem. C 2010, 114, 2694-2700.

[12] L. Li, P. Hua, X. Tian, C. Yang and Z. Pi, Electrochim. Acta 2010, 55, 1682-1686.

[13] F. Jiao, J. C. Jumas, M. Womes, A. V. Chadwick, A. Harrison and P. G. Bruce, J. Am. Chem. Soc. 2006, 128, 12905-12909.

[14] H. Tüysüz, Y. J. Hwang, S. B. Khan, A. M. Asiri and P. Yang, Nano Res. 2013, 6, 47-54.

[15] Z. Wu, Q. Li, D. Feng, P. A. Webley and D. Zhao, J. Am. Chem. Soc. 2010, 132, 12042-12050.

[16] E. Kang, S. An, S. Yoon, J. K. Kim and J. Lee, J. Mater. Chem. 2010, 20, 7416-7421.

[17] B. P. Bastakoti, Y. Li, T. Kimura and Y. Yamauchi, Small 2015, 11, 1992-2002.

[18] P. Yang, D. Zhao, D. I. Margolese, B. F. Chmelka and G. D. Stucky, Nature 1998, 396, 152.

[19] N. Suzuki, M. Imura, Y. Nemoto, X. Jiang and Y. Yamauchi, CrystEngComm, 2011, 13, 40-43.

[20] X. Jiang, N. Suzuki, B. P. Bastakoti, K. C. W. Wu and Y. Yamauchi, Chem. Asian J. 2012, 7, 1713-1718.

[21] S. Tanaka, B. P. Bastakoti, S.-I. Yusa, D. Ishii, K. Kani, A. Fatehmulla, W. A. Farooq, M. J. A. Shiddiky, Y. Bando, Y. V. Kaneti, Y. Yamauchi and M. S. A. Hossain, Eur. J. Inorg. Chem. 2017, 2017, 1328-1332.

[22] S. Tanaka, Y. V. Kaneti, R. Bhattacharjee, M. N. Islam, R. Nakahata, N. Abdullah, S.-I. Yusa, N.-T. Nguyen, M. J. A. Shiddiky, Y. Yamauchi and M. S. A. Hossain, ACS Appl. Mater. Interfaces 2018, 10, 1039-1049.

[23] X. Lai, G. Shen, P. Xue, B. Yan, H. Wang, P. Li, W. Xia and J. Fang, Nanoscale 2015, 7, 4005-4012.

[24] D. Luo, Y.-P. Deng, X. Wang, G. Li, J. Wu, J. Fu, W. Lei, R. Liang, Y. Liu, Y. Ding, A. Yu and Z. Chen, ACS Nano 2017, 11, 11521-11530.

[25] J. He, M. Wang, W. Wang, R. Miao, W. Zhong, S.-Y. Chen, S. Poges, T. Jafari, W. Song, J. Liu and S. L. Suib, ACS Appl. Mater. Interfaces 2017, 9, 42676-42687.

[26] Y. G. Wang and Y. Y. Xia, Electrochim. Acta 2006, 51, 3223-3227.

[27] F. Jiao, A. H. Hill, A. Harrison, A. Berko, A. V. Chadwick and P. G. Bruce, J. Am. Chem. Soc. 2008, 130, 5262-5266.

[28] H. Liu, G. Wang, J. Liu, S. Qiao and H. Ahn, J. Mater. Chem. 2011, 21, 3046-3052.

[29] W. Xing, F. Li, Z.-F. Yan and G. Q. Lu, J. Power Sources 2004, 134, 324-330.

[30] S. Vijayakumar, S. Nagamuthu and G. Muralidharan, ACS Appl. Mater. Inter. 2013, 5, 2188-2196.

[31] J. Min, J. Liu, M. Lei, W. Wang, Y. Lu, L. Yang, Q. Yang, G. Liu and N. Su, ACS Appl. Mater. Inter. 2016, 8, 780-791.

[32] X. Wang, L. Sun, X. Sun, X. Lid and D. He, Mater. Res. Bull. 2017, 96, 533-537.

[33] G. Bai, H. Dai, J. Deng, Y. Liu and K. Ji, Catal. Commun. 2012, 27, 148-153.

[34] F. Yu, X. Xu, H. Peng, H. Yu, Y. Dai, W. Liu, J. Ying, Q. Sun and X. Wang, Appl. Catal. A Gen. 2015, 507, 109-118.

[35] X. Song, L. Gao and S. Mathur J. Phys. Chem. C 2011, 115, 21730-21735.

[36] Y. Ding, Y. Wang, L. Su, H. Zhang and Y. Lei, J. Mater. Chem. 2010, 20, 9918-9926.

Figures and Figure Captions

Figure 1 Synthesis route of PS_{402}-*b*-PAA_{71}-*b*-PEG_{46}.

Figure 2 (a) TEM image of PS_{402}-*b*-PAA_{71}-*b*-PEG_{46} in pure water at C_p = 0.2 g L^{-1}. (b) Diameter distribution histogram of the polymeric micelles.

Figure 3 Schematic illustration showing the mechanism of the formation of mesoporous NiO using the PS-b-PAA-b-PEG triblock copolymer template.

Figure 4 (a, c, e) SEM images and (b, d, f) the corresponding pore diameter distributions of mesoporous NiO obtained using different amounts of nickel salt: (a) 10 mg (0.0344 mmol), (b) 20 mg (0.0688 mmol), and (c) 30 mg (0.1032 mmol).

Figure 5 SEM images of the mesoporous NiO obtained at (a) 250 °C, (b) 350 °C, and (c) 450 °C.

Figure 6 (a) TEM and (b) high-resolution TEM (HRTEM) images of mesoporous NiO obtained at an optimized calcination temperature of 350 °C. (inset of (b): selected area electron diffraction (SAED)).

Figure 7 TG curves of (a) PS-b-PAA-b-PEG triblock copolymer and (b) PS-b-PAA-b-PEG micelles (with Ni^{2+}). (c) Wide-angle XRD patterns for mesoporous NiO obtained at different calcination temperatures and (d) N_2 adsorption-desorption isotherms of mesoporous NiO obtained at the optimized calcination temperature of 350 °C.

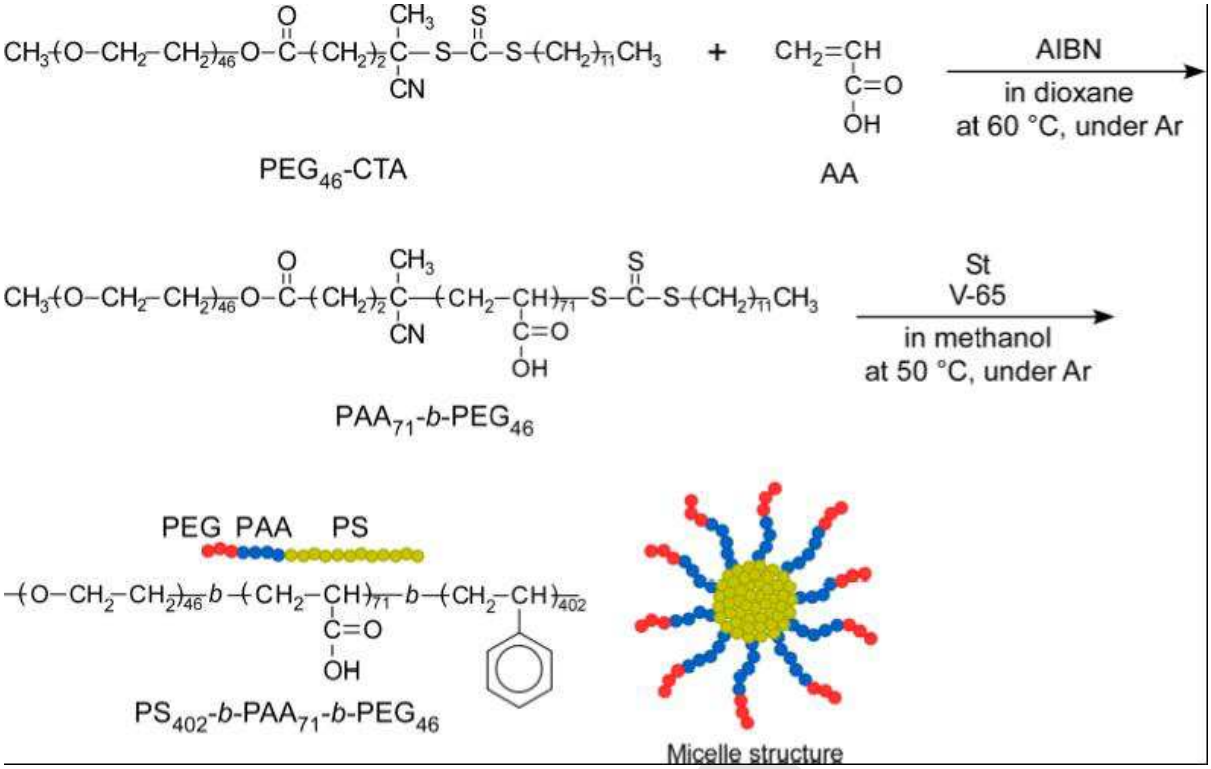

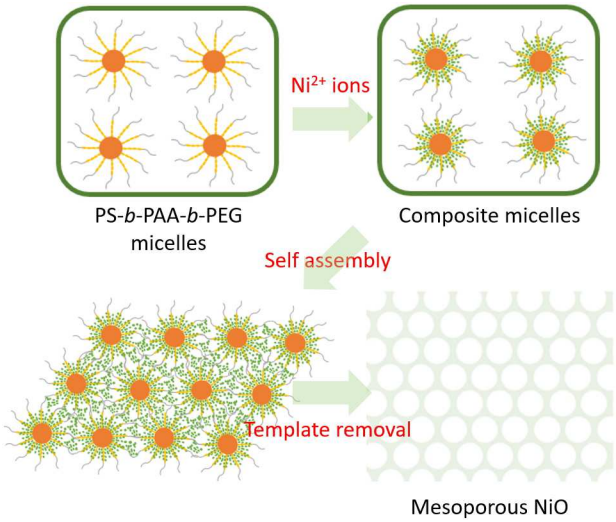

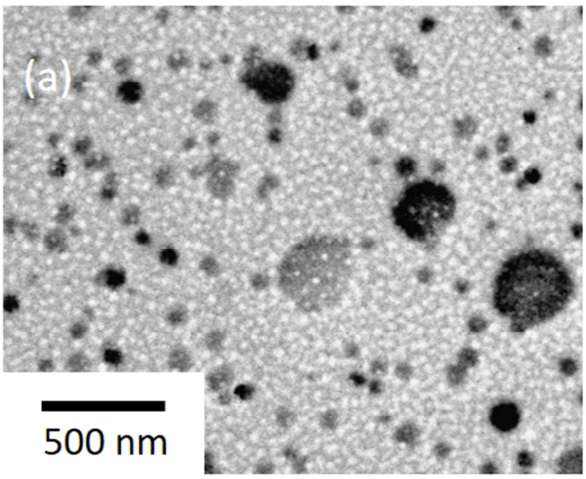

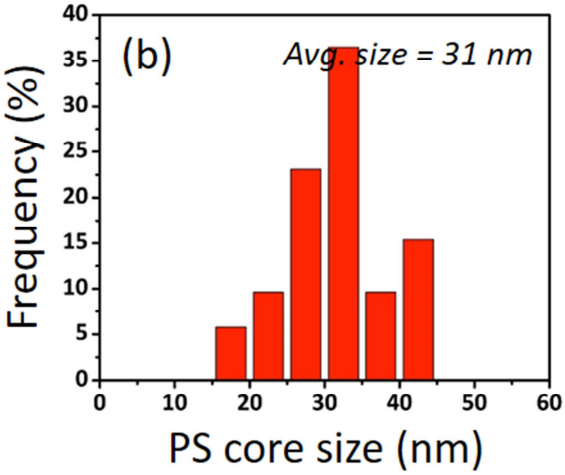

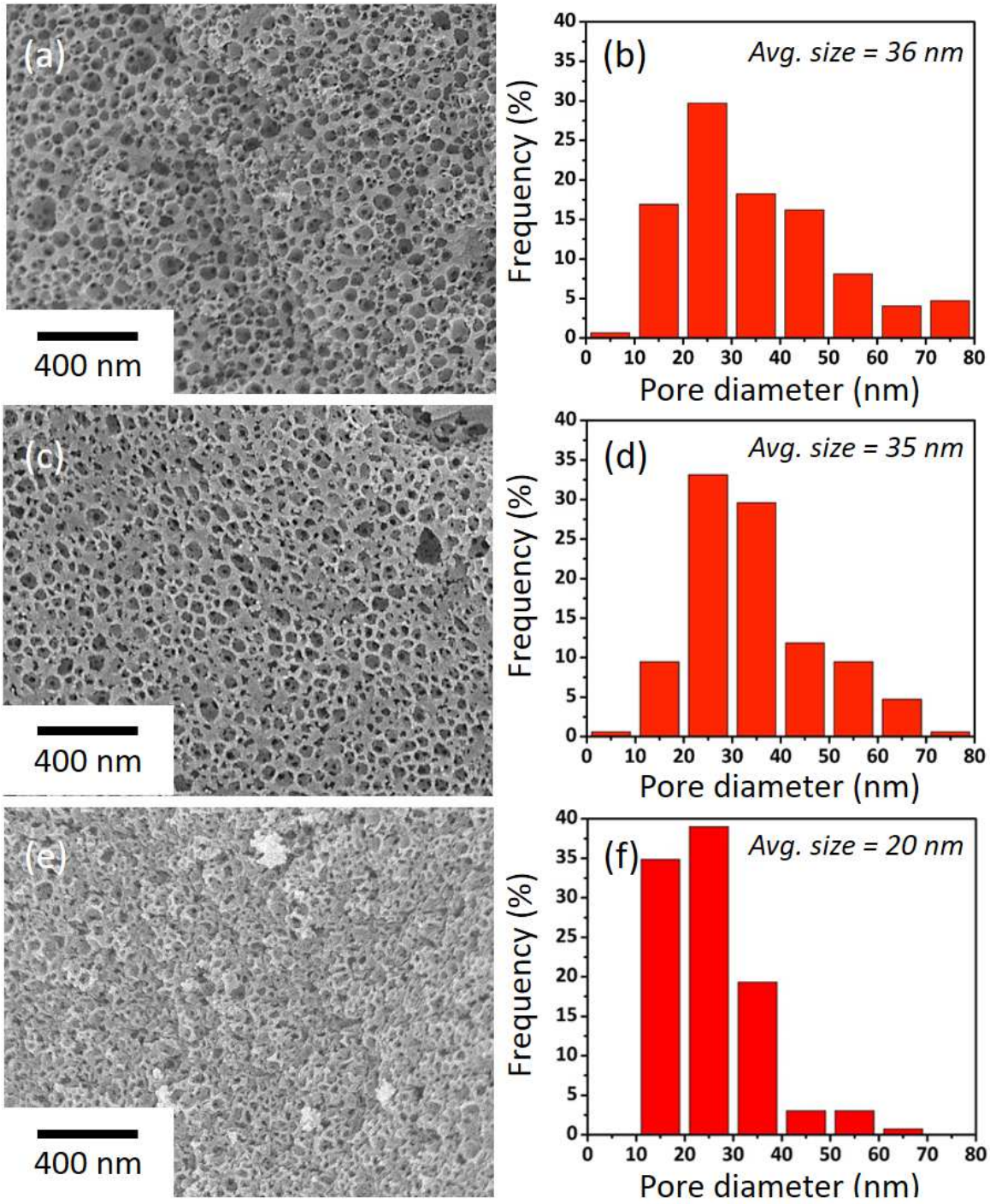
(a)
400 nm
(b)
Avg. size = 36 nm
Frequency (%)
Pore diameter (nm)
(c)
400 nm
(d)
Avg. size = 35 nm
Frequency (%)
Pore diameter (nm)
(e)
400 nm
(f)
Avg. size = 20 nm
Frequency (%)
Pore diameter (nm)

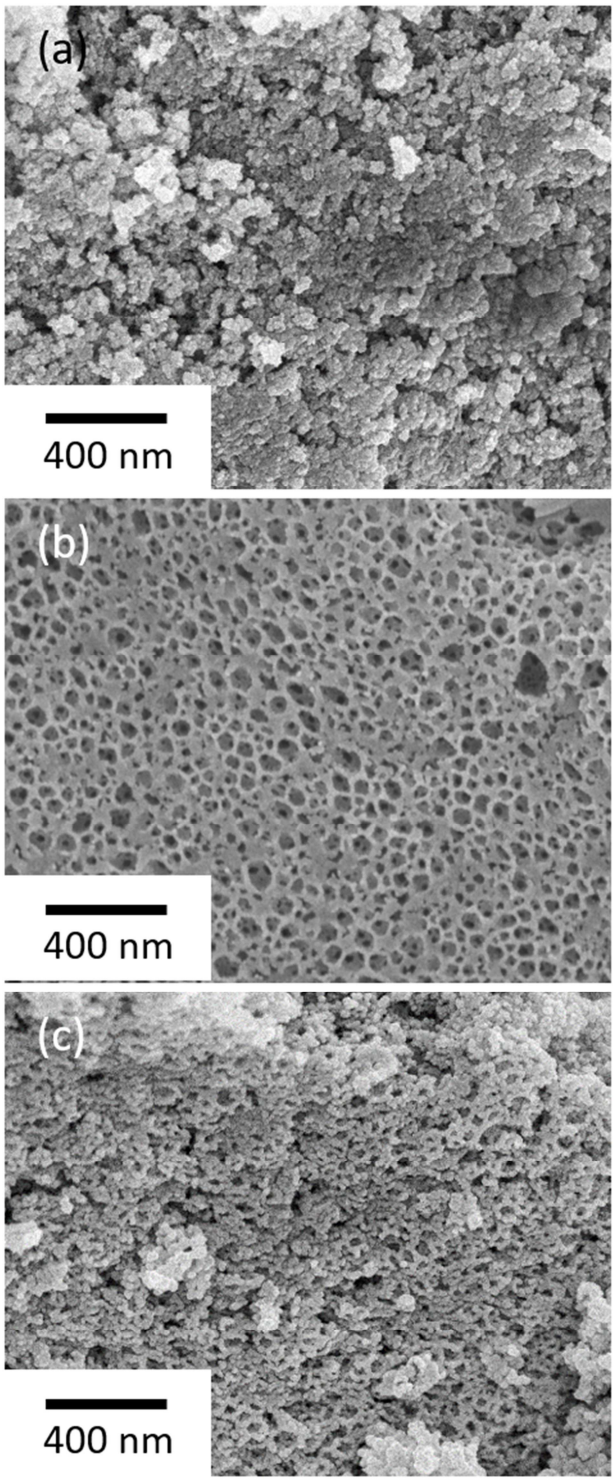

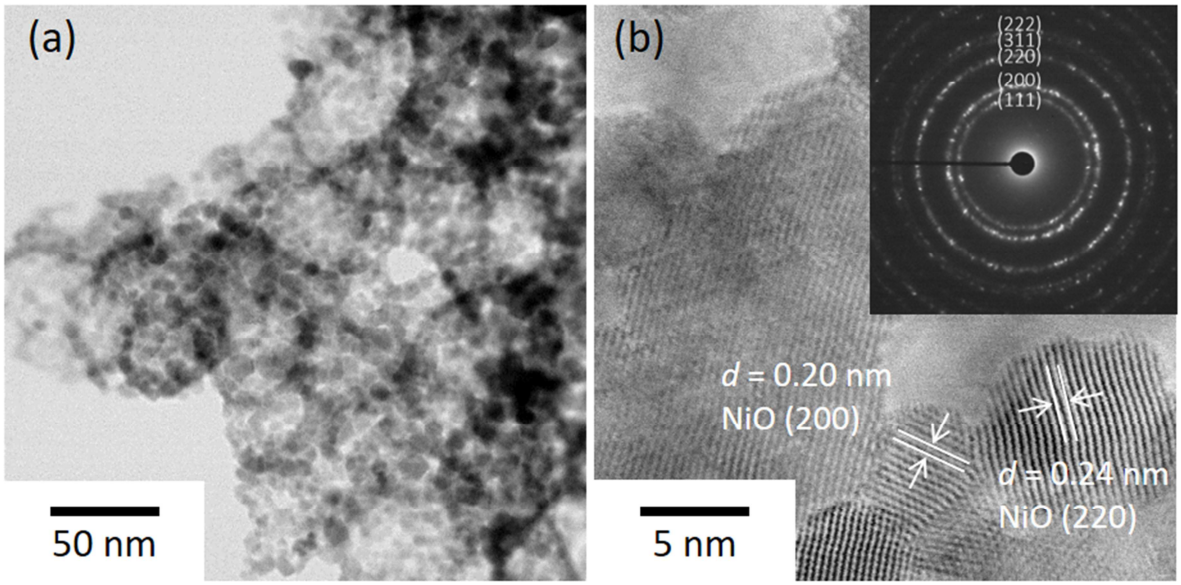

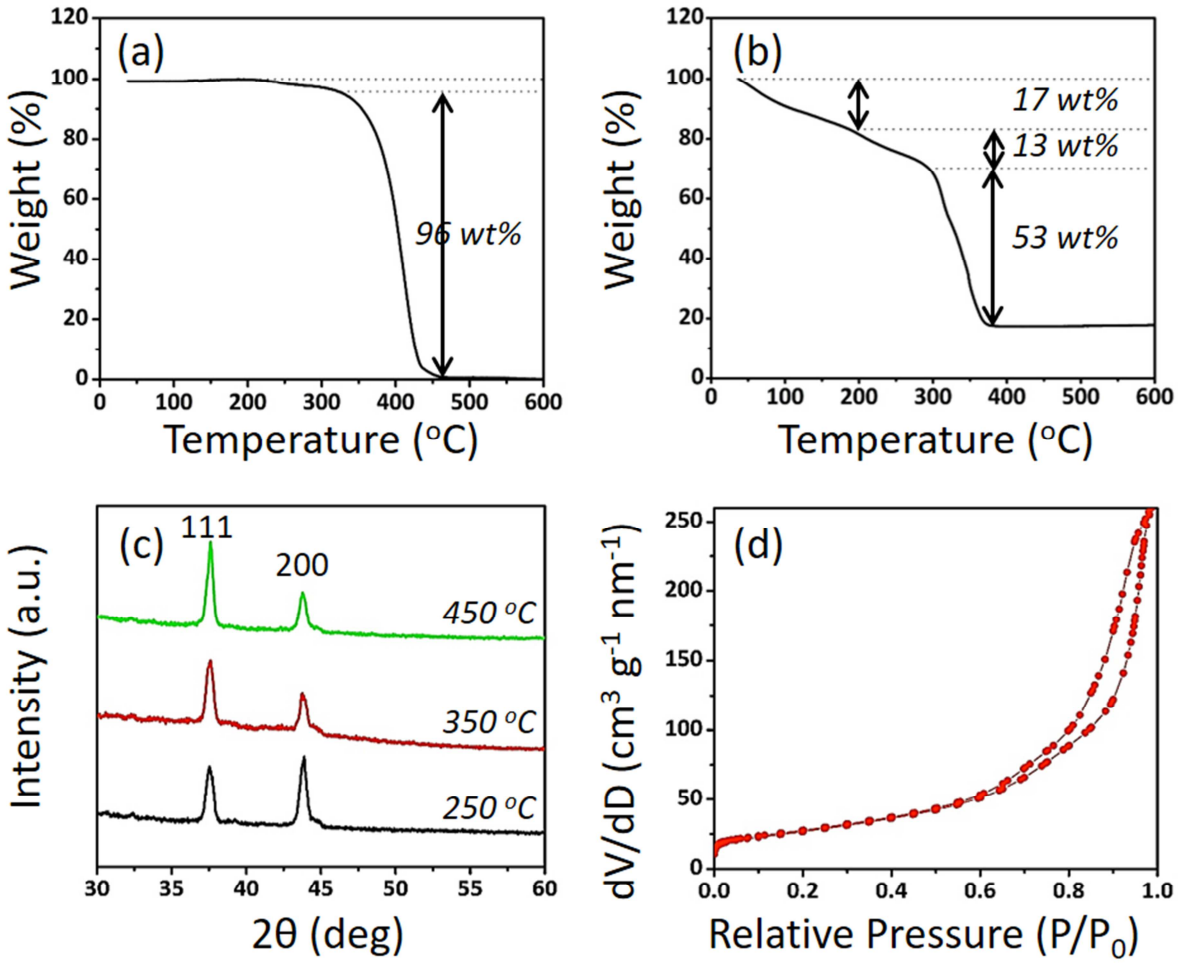
(a)
Weight (%)
Temperature (°C)
96 wt%
(b)
17 wt%
13 wt%
53 wt%
(c)
111
200
450 °C
350 °C
250 °C
Intensity (a.u.)
2θ (deg)
(d)
dV/dD (cm³ g⁻¹ nm⁻¹)
Relative Pressure (P/P0)

Highlights

- Asymmetric poly(styrene-block-acrylic acid-block-ethylene glycol) (PS-b-PAA-b-PEG) triblock copolymer has been synthesized and used as soft-template.
- The soft template was achieved by micelle formation from PS core, a PAA shell and a PEG corona in aqueous solutions.
- The synthesized mesoporous NiO exhibits a large average pore size of 35 nm with large specific surface area and pore volume of 97.0 $m^2 g^{-1}$ and 0.411 $cm^3 g^{-1}$, respectively.